Partial volume correction of brain perfusion estimates using the inherent signal data of time-resolved arterial spin labeling.

Ahlgren, André; Wirestam, Ronnie; Petersen, Esben Thade; Ståhlberg, Freddy; Knutsson, Linda

Published in:
NMR in Biomedicine

DOI:
10.1002/nbm.3164

2014

Partial Volume Correction of Brain Perfusion Estimates Using the Inherent Signal Data of Time-Resolved Arterial Spin Labeling

André Ahlgren (1), Ronnie Wirestam (1), Esben Thade Petersen (2), Freddy Ståhlberg (1,3) and Linda Knutsson (1)

(1) Department of Medical Radiation Physics, Lund University, Lund, Sweden
(2) Department of Radiology, University Medical Center Utrecht, Utrecht, The Netherlands
(3) Department of Diagnostic Radiology, Lund University, Lund, Sweden

Corresponding author:

André Ahlgren
E-mail address: Andre.Ahlgren@med.lu.se
Telephone: +46 46-173146
Fax: +46 46-178540
Address:
Department of Medical Radiation Physics
Lund University
Barngatan 2B
Skåne University Hospital, Lund
SE-221 85 LUND
Sweden

Word count: 6253
Number of figures: 6
Number of tables: 1
Number of references: 29
Number of supplementary material files: 2

Keywords: partial volume correction, partial volume effect, perfusion, arterial spin labeling, brain segmentation, fractional signal modelling, QUASAR, FRASIER

Abstract

Quantitative perfusion MRI based on arterial spin labeling (ASL) is hampered by partial volume effects (PVE), arising due to voxel signal cross-contamination between different compartments. To address this issue, several partial volume correction (PVC) methods have been presented. Most previous methods rely on segmentation of a high-resolution T1-weighted morphological image volume that is coregistered to the low-resolution ASL data, making the result sensitive to errors in the segmentation and coregistration. In this work, we present a methodology for partial volume estimation and correction, using only low-resolution ASL data acquired with the QUASAR sequence. The methodology consists of a T1-based segmentation method, with no spatial priors, and a modified PVC method based on linear regression. The presented approach thus avoids prior assumptions about the spatial distribution of brain compartments, while also avoiding coregistration between different image volumes. Simulations based on a digital phantom as well as in vivo measurements in 10 volunteers were used to assess the performance of the proposed segmentation approach. The simulation results indicated that QUASAR data can be used for robust partial volume estimation, and this was confirmed by the in vivo experiments. The proposed PVC method yielded probable perfusion maps, comparable to a reference method based on segmentation of a high-resolution morphological scan. Corrected gray matter (GM) perfusion was 47% higher than uncorrected values, suggesting a significant amount of PVEs in the data. Whereas the reference method failed to completely eliminate the dependence of perfusion estimates on the volume fraction, the novel approach produced GM perfusion values independent of GM volume fraction. The intra-subject coefficient of variation of corrected perfusion values was lowest for the proposed PVC method. As shown in this work, low-resolution partial volume estimation in connection with ASL perfusion estimation is feasible, and provides a promising tool for decoupling perfusion and tissue volume.

List of abbreviations

AIF	arterial input function
ASL	arterial spin labeling
CBF	cerebral blood flow
COV	coefficient of variation
CSF	cerebrospinal fluid
GM	gray matter
PVC	partial volume correction
PVE	partial volume effect
SNR	signal-to-noise ratio
VA	volume agreement
VO	volume overlap
WM	white matter

Introduction

Arterial spin labeling (ASL) is a functional MRI method characterized by non-invasive quantification and spatial mapping of perfusion, accomplished by magnetically inverting arterial blood water upstream to the regions of interest (1,2). When studying the brain, the corresponding measured physical quantity is referred to as the cerebral blood flow (CBF), traditionally reported in units of ml blood per 100 g tissue per minute [ml/100g/min]. A single ASL signal acquisition has a low sensitivity to perfusion and, to accommodate this, the experiment is often realized using low spatial resolution and averaging of signal data from several repetitions. The low resolution makes the estimated perfusion values sensitive to the partial volume effect (PVE) (3), i.e., perfusion values may be unreliable due to signal contribution from several compartments within a single voxel. Note that, in the case of, for example, positron emission tomography, PVEs also emerge due to the large (compared to the voxel size) point spread function (4,5). The PVE has a large impact on absolute perfusion quantification in human brain tissue, and potentially also to relative measurements, for example, in thin cortical tissue. It is of considerable importance to either correct for or identify any dependence on the PVE of the measured parameters, especially when studying diseases in which a volumetric tissue alteration is plausible, e.g., cerebral atrophy in elderly or in connection with neurodegenerative diseases.

Multiple methods for correction of PVEs, i.e., partial volume correction (PVC), have been proposed in the literature (4-11). For CBF quantification with ASL, most methods rely on segmentation of the brain into a number of compartments (tissue types), normally gray matter (GM), white matter (WM) and cerebrospinal fluid (CSF). This is often accomplished by an automatic segmentation routine using signal intensities from a separate high-resolution T1-weighted image volume, followed by a spatial coregistration of the segmentation results to the ASL image. This approach may be sufficient in many cases, but the coregistration step can also prove to be difficult, especially when the two datasets are based on substantially different imaging protocols (e.g., read-out technique, resolution and contrast). Resulting maps are often probability maps consisting of floating point values between 0 and 1, and it is common to regard these as tissue partial volume estimates. However, probability maps contain estimates of the probability that a voxels consists purely of a certain compartment, and the use of probability values as partial volume estimates in PVC algorithms may thus not be strictly correct. If the perfusion and segmentation maps are spatially aligned, mean CBF values can be calculated in binary tissue masks, where the threshold for the masks are set to minimize PVEs, or a model of the partial volume effect can be applied to infer unperturbed perfusion values.

Asllani et al. (7) modeled the measured perfusion signal in a voxel as the linear sum of the signal contribution from GM, WM and CSF. They used spatial linear regression, i.e., assuming that the underlying perfusion remained constant in the local region around each voxel, thereby solving the otherwise underdetermined equation system at the cost of spatial blurring. The results were promising, but it is clear that such an approach relies heavily on the coregistered tissue probability maps, obtained from segmentation of a high-resolution structural image. Chappell et al. (8) proposed the use of non-linear Bayesian inference to correct for PVEs in time-resolved (multi-TI) ASL. The methodology and results were comparable to the linear regression approach, although spatial details in the corrected CBF maps were preserved to greater extent through the use of adaptive spatial priors. In a similar attempt to reduce the inherent blurring of linear least squares, Liang et al. (11) proposed the use of least trimmed squares regression. Although all of the studies referred to above (7,8,11) used a separate high-resolution structural scan for PVC, neither of the respective PVC

algorithms are intrinsically dependent on that particular type of partial volume estimates. Recently, Petr et al (9) applied the PVC method by Asllani et al. (7) to multi-TI ASL data, using a separate low-resolution Lock-Locker EPI sequence for partial volume estimation. Even though this reduced the differences between the two imaging protocols, coregistration between segmentation data and ASL data was employed.

To avoid the problems associated with available methods, we demonstrate the implementation of segmentation and partial volume correction in the native space of low-resolution ASL images, through the use of quantitative T1 mapping. This was accomplished within the framework of model-free ASL, solely exploiting the data collected with the QUASAR pulse sequence (12). To the best of our knowledge, this is the first study to demonstrate the extraction of partial volume estimates from the same dataset as the perfusion estimates, thus avoiding the need for any additional scans or coregistration. The performance of the proposed segmentation method was assessed through simulations and validated in vivo. PVC was applied to in vivo data using a modified linear regression approach, exploiting the novel segmentation approach. For comparison, PVC was also performed using an established segmentation method based on a high-resolution morphological image dataset.

Theory

Signal Modeling

Using the QUASAR sequence (12), time-resolved ASL data are acquired using a saturation recovery Look-Locker read-out. Hence, the raw data (i.e., before subtraction) follows an exponential saturation recovery with a limiting value being the effective equilibrium tissue magnetization, given by (13):

$$M_{0t,eff} = M_{0t} \cdot \frac{1 - e^{-\frac{\Delta TI}{T_{1t}}}}{1 - \cos(\phi)\, e^{-\frac{\Delta TI}{T_{1t}}}} \quad [1]$$

where M_{0t} is the equilibrium tissue magnetization, ΔTI is the time between excitation pulses, T_{1t} is the longitudinal tissue relaxation time, and ϕ is the flip angle. Due to the repeated excitation pulses, the recovery follows an effective longitudinal relaxation time which relates to T_{1t} through:

$$\frac{1}{T_{1t,eff}} = \frac{1}{T_{1t}} - \frac{\ln(\cos(\phi))}{\Delta TI} \quad [2]$$

Both $M_{0t,eff}$ and $T_{1t,eff}$ can be estimated on a voxel-by-voxel basis by fitting the saturation recovery signal equation to the signal propagation of the raw ASL data:

$$S(t) = M_{0t,eff}\left(1 - A \cdot e^{-t/T_{1t,eff}}\right) \quad [3]$$

where A is a fitting parameter and t is the saturation time (i.e., time between saturation preparation and read-out). When $M_{0t,eff}$ and $T_{1t,eff}$ have been estimated, the true M_{0t} and T_{1t} can be calculated using Eqs. 1 and 2.

For accurate calculation of M_{0t} and T_{1t}, the local effective flip angle ϕ needs to be determined according to:

$$\phi = \phi_n \cdot g \quad [4]$$

where ϕ_n is the nominal flip angle and g is a spatially varying B1 correction factor. The dual flip angle strategy (14) enables the estimation of g by minimizing

$$\frac{1}{T_{1t,eff,low}} + \frac{\ln\left(\cos\left(\phi_{n,low} \cdot (g + \Delta g)\right)\right)}{\Delta TI} - \left(\frac{1}{T_{1t,eff,high}} + \frac{\ln\left(\cos\left(\phi_{n,high} \cdot g\right)\right)}{\Delta TI}\right) \quad [5]$$

for g, where indices 'low' and 'high' indicate the two different flip angles. The slice-profile effects vary slightly with flip angle in a 2D acquisition and this is accounted for by the correction Δg=0.023 (14). Details regarding estimation of T_{1t} and M_{0t} from QUASAR data have been reported previously (14,15).

Segmentation

The saturation recovery signal acquisition inherent to the QUASAR sequence can be used to perform an automatic brain segmentation based on quantitative T1 mapping (16). This segmentation principle was adopted from the FRASIER method proposed by Shin et al. (17).

The measured signal in a voxel is modelled as a linear combination of CSF, GM and WM, each with unique and well-defined magnetization and relaxation properties:

$$S(t) = \sum_i \left[f_{s,i} M_{ss,i} \left(1 - A \cdot e^{-t/T_{1,i,eff}}\right)\right] \quad [6]$$

where i represents the respective compartment, $f_{s,i}$ is the corresponding fractional signals, and

$$M_{ss,i} = \frac{1 - e^{\Delta TI/T_{1,i}}}{1 - \cos(\phi) \cdot e^{\Delta TI/T_{1,i}}} \quad [7]$$

corrects for the incomplete steady state of the equilibrium magnetization of compartment i. For a discrete set of N signal values $\mathbf{S_m} = [\, S(t_1) \ \ldots \ S(t_N)]^T$, Eq. 6 can be written in matrix form as

$$\mathbf{S_m} = \mathbf{X} \cdot \mathbf{F_s} \quad [8]$$

where

$$X_{j,i} = M_{ss,i}\left(1 - A \cdot e^{-t_j/T_{1t,eff,i}}\right), \ \ 1 \le j \le N \quad [9]$$

and

$$\mathbf{F_s} = \left[\, f_{s,CSF} \ \ f_{s,GM} \ \ f_{s,WM} \,\right]^T \quad [10]$$

With this formulation, $\mathbf{F_s}$ can be estimated by means of linear least squares estimation, i.e., $\mathbf{F_s} = (\mathbf{X}^T\mathbf{X})^{-1}\mathbf{X}^T\mathbf{S_m}$, where $(\mathbf{X}^T\mathbf{X})^{-1}\mathbf{X}^T$ is the pseudo-inverse of $\mathbf{X}$. The fractional volume $f_{v,i}$ (partial volume estimate) can be calculated by division of the fractional signal by the water content ρ_{wc} of the respective compartment:

$$f_{v,i} = \frac{f_{s,i}}{\rho_{wc,i}} \quad [11]$$

The fractional volumes are constrained by $\sum_i f_{v,i} = 1$ to obtain normalized values.

Perfusion Quantification

Perfusion quantification in model-free ASL is based on the general kinetic equation (18) and employs deconvolution of the time-resolved perfusion signal, $\Delta M(t)$, and the corresponding arterial input function (AIF) according to:

$$\Delta M(t) = 2 \cdot M_{0a} \cdot CBF \cdot [c(t) \otimes R(t)] \quad [12]$$

where "⊗" denotes convolution, $M_{0,a}$ is the magnetization of fully relaxed arterial blood, $c(t)$ is the fractional AIF and $R(t)$ is the effective impulse residue function (including effects of wash-out and relaxation). The QUASAR sequence employs crusher gradients to obtain arterial signal curves and absolute AIFs are defined as $C_{AIF}(t) = 2 \cdot M_{0,a} \cdot c(t)$, so that deconvolution yields the perfusion-scaled residue function $CBF \cdot R(t)$. Deconvolution was performed using oscillation index truncated block-circulant singular value decomposition (19). The theory of model-free ASL is explained in detail by Petersen et al. (12,14,20).

Partial volume correction

Partial volume correction was achieved through a simplification of the linear regression method proposed by Asllani et al. (7). Since QUASAR perfusion estimation is based on model-free quantification, we chose to perform PVC directly on the CBF maps (rather than the ASL difference maps). Hence, the measured CBF was modeled as:

$$CBF = \sum_i \left[f_{v,i} \cdot CBF_i \right] \quad [13]$$

where CBF_i is the unknown underlying perfusion contribution of compartment i, to the total perfusion, and partial volumes act as weighting factors. It was assumed that CSF does not contribute to the perfusion signal, i.e., $CBF_{CSF} = 0$. Estimation of $\mathbf{CBF_t} = [CBF_{GM}, CBF_{WM}]^{\mathrm{T}}$ from Eq. 13 is not possible in a single voxel since the equation is underdetermined. By assuming that partial-volume-free perfusion in GM and WM does not vary in a local region, more data are included and the corresponding equation system can be solved. In contrast to the square regression kernel commonly used in spatial linear regression, we define the local region based on Euclidian distance by using a circular regression kernel. Hence, at voxel position $\mathbf{r}_k = (x_k, y_k)$ we assume that $\mathbf{CBF_t}(\mathbf{r}_k) = \mathbf{CBF_t}(\mathbf{r}_n)$ for all neighboring voxels at position $\mathbf{r}_n$ that satisfy $\|\mathbf{r}_n - \mathbf{r}_k\| \leq R$, where R is the radius of the circular kernel. The parameters of interest can be estimated by linear regression:

$$\mathbf{CBF}(\mathbf{r}_k) = \mathbf{F_v}(\mathbf{r}_k) \cdot \mathbf{CBF_t}(\mathbf{r}_k) \quad [14]$$

where $\mathbf{CBF}(\mathbf{r}_k)$ is the column vector of measured perfusion values included in the regression kernel centered at $\mathbf{r}_k$, and $\mathbf{F_v}(\mathbf{r}_k)$ is the matrix with the corresponding estimated fractional volumes (two columns since we can ignore the zero term originating from CSF). Hence, CBF_{GM} and CBF_{WM} can be estimated through conventional linear least-squares analysis, i.e., $\mathbf{CBF_t} = (\mathbf{F_v}^T \mathbf{F_v})^{-1} \mathbf{F_v}^T \mathbf{CBF}$, where $(\mathbf{F_v}^T \mathbf{F_v})^{-1} \mathbf{F_v}^T$ is the pseudo-inverse of $\mathbf{F_v}$. Although the analysis yields estimation of both GM and WM perfusion, we will focus on GM perfusion in this work. Estimation of absolute WM perfusion with ASL is challenging, primarily due to a low absolute perfusion levels and prolonged blood arrival time, compared to GM, and it has been suggested that a large amount of repetitions are needed for reliable WM results (21).

The PVC analysis can be used to produce partial tissue perfusion maps $pCBF_{GM} = f_{v,GM} \cdot CBF_{GM}$, and/or partial-volume-free tissue perfusion maps CBF_{GM}. There is some variety in the interpretation of PVC of perfusion maps, where either $pCBF_{GM}$ or CBF_{GM} is referred to as

partial-volume-corrected GM perfusion. These two definitions actually originate from two different ways of acknowledging PVEs. The former interpretation highlights that the PVE is a loss of contrast due to a mixture of tissues in a single voxel, and the PVC is used to 'clean' the perfusion map from, in this case, contributions from WM. Partial tissue perfusion maps may also be added together (e.g., $pCBF_{GM+WM} = pCBF_{GM} + pCBF_{WM}$), yielding a type of denoised version of the measured CBF map which reintroduces the PVEs (9). Note that the $pCBF_{GM}$ value can be misleading since it does not reflect the underlying perfusion of the GM, but rather the contribution to the voxel CBF estimate originating from the GM within that voxel (which has little physiological meaning). For very low resolution, such as in ASL experiments, we have reason to believe that very few voxels contain 100% GM, and the latter interpretation of PVC, i.e., producing partial-volume-free tissue perfusion maps, aims at completely removing the dependence on tissue volume. This approach yields visually unnatural maps of GM perfusion, with no morphological information, but can be of importance when decoupling of regional or global changes in perfusion from changes in tissue volume is warranted, for example, in the case of atrophy. In this work, we analyze $pCBF_{GM}$ and CBF_{GM} separately.

Methods

MRI Experiments

Data from ten volunteers (6 males, 4 females, age 21-65 years) participating in the multi-center QUASAR study (20), were used. Each volunteer was scanned four times with the QUASAR sequence resulting in a total of 40 data sets. The scans were divided into two sessions, where one session included repositioning between the ASL acquisitions and the other session was performed without repositioning. The study was approved by the local ethics committee, and all volunteers gave written informed consent. The experiments were performed on a 3T MRI unit (Philips Achieva, Philips Healthcare, Best, The Netherlands) using an 8-channel SENSE receiver head coil. For the QUASAR acquisition, the following parameters were used: TR/TE/ΔTI/TI_1=4000/23/300/40 ms, 35°/11.7° flip angles, 640 ms bolus length, 13 inversion times, 84 series (48 crushed, 24 non-crushed and 12 low flip angle - alternating label and control), 4 cm/s velocity encoding for the crushed pairs, 150 mm labeling thickness, 7 slices, 6 mm slice thickness, 2 mm slice gap, 64×64 matrix, 3.75×3.75 mm^2 in-plane resolution, SENSE factor 2.5, at a total scan time of 5 min 52 s. A high-resolution morphological scan (MPRAGE) was acquired using the following parameters: TR/TE=6.7/3.1 ms, TI=0.8 s, FA=8°, voxel size=0.9×0.9×0.9 mm^3, 288×288 matrix, 80 slices with a scan duration of 5 min 26 s. In the session without repositioning, only one MPRAGE scan was performed. Automatic planning was achieved using the SmartExam software (20,22).

Simulations

The proposed segmentation methodology was validated through simulations based on a high-resolution (1 mm isotropic) digital phantom of a normal brain from BrainWeb (23) [http://brainweb.bic.mni.mcgill.ca/brainweb/], composed by tissue fractions of CSF, GM and WM. The tissue maps were down-sampled (by averaging over neighboring voxels) to the same resolution as the QUASAR data and used as ground truth in the simulations. Simulated MR signal sampling was generated based on Eqs. 6 and 7, using the same parameters as in the in vivo experiments. T_{1t} was set to 1.5, 1.0 and 4.3 s for GM, WM and CSF, respectively, and $T_{1t,eff}$ was calculated from Eq. 2. Water content and g was set to one in the simulations.

Gaussian noise was added corresponding to signal-to-noise ratio (SNR) levels ranging from 25 to 200, where SNR was defined as the signal intensity at steady state (M_{0t}) divided by the standard deviation of the added noise. The multiple repetitions in the QUASAR sequence allowed the same SNR measure to be estimated in vivo. The down-sampled digital phantom consisted of 7,726 voxels and the simulation was repeated 10 times yielding a total of 77,260 simulated signal curves per SNR level. The segmentation was performed according to the descriptions in the 'Theory' and 'Post-processing' sections. PVC of ASL data using linear regression has been simulated and evaluated elsewhere (7-9), and was not included in the simulations.

Post-processing

All post-processing was executed on a PC using MATLAB 2012a (The MathWorks, Inc., Natick, MA, USA) using in-house written software (unless stated otherwise), based on the theory presented above, as well as in Refs. (12,17).

Segmentation

Both the true and the effective relaxation times for the three compartments need to be determined (see Eqs. 6 and 7) prior to the segmentation. The true relaxation times for GM and WM were estimated as the mean values in a multiple Gaussian distribution fit on the whole brain T_{1t} histogram. Shin et al. estimated the effective relaxation times from a whole brain histogram (17), whereas we chose to calculate it voxel-wise as

$$\frac{1}{T_{1t,eff,i}} = \frac{1}{T_{1t,i}} - \frac{\ln(\cos(\phi))}{\Delta TI} \qquad [15]$$

The motivation for this approach was that we acquired estimates of the local flip angle, and, consequently, $M_{ss,i}$ becomes a parametric map in our implementation. It is difficult to achieve a robust estimation of the relaxation time in CSF, mainly due to few voxels and excessive PVE, and a fixed literature value of 4.3 s was used in this study (17). Water contents (ρ_{wc}) of 100%, 89% and 73% were used for CSF, GM and WM, respectively (24). To reduce the signal contribution from arterial blood, only the crushed QUASAR data were used in the segmentation routine. Segmentation of MPRAGE data was performed using the 'New Segment' routine in SPM8 [http://www.fil.ion.ucl.ac.uk/spm/], which is an extension of the default unified segmentation routine (25). This routine is based on Gaussian mixture modeling of the MR signal and performs best on a high-resolution anatomical scan.

Perfusion Quantification

QUASAR data were analyzed with the EasyMRI software, developed by Esben Petersen. The automatic routines produced maps of CBF, arterial blood volume, arterial transit time and longitudinal relaxation rate (R1), of which only CBF and R1 were used in this study.

Partial Volume Correction

The radius of the circular kernel in the PVC routine must be set by the user. To ensure that the overall results were not heavily dependent on the selected kernel radius, analysis was performed for integer radii ranging from 2 to 6 voxels (see Supplementary Material 1). For the continued analysis, a radius of 3 voxels was employed yielding a total of 37 voxels. This was found to be a reasonable trade-off between the degree of smoothing and the amount of voxels for which $\mathbf{F_v}(\mathbf{r}_k)$ was singular. Any center voxels for which the fractional volume matrix was singular was omitted from further analysis.

The proposed PVC approach, based on segmentation of QUASAR data, can be applied immediately after the mapping of CBF and partial volumes. This approach is referred to as PVC-QUASAR in this work. The high-resolution segmentation maps produced by SPM8, on the other hand, need to be coregistered to the ASL space before applying the PVC routine. A conventional approach with spline interpolation generally yields non-ideal results for coregistration between images with very different spatial resolutions, and therefore we applied the methodology described by Chappell et al. (8). In short, the R1 map from the QUASAR software was super-sampled to the same in-plane spatial resolution as the MPRAGE, and used as a fixed reference. The MPRAGE volume was then coregistered to the supersampled ASL volume using a 12 parameter affine transform, and the same transform was applied to the segmentation maps. Integration over the coregistered segmentation maps yielded low-resolution partial volume maps in ASL space. Note that the 'Coregister' routine in SPM8 [http://www.fil.ion.ucl.ac.uk/spm/] uses a default 6 parameter (translation and rotation) rigid body transform (26). Since the ASL data and the high-resolution MPRAGE data may have different geometrical distortions due to different readout schemes, we modified the routine to allow for a 12 parameter affine transform, i.e., including scaling and shearing (John Ashburner, personal communication). The PVC approach based on segmentation of MPRAGE data is referred to as PVC-MPRAGE below.

Analysis

Segmentation Assessment

The accuracy and precision of the simulated segmentation was calculated for each compartment as

$$Accuracy_i = \sum_j (f^*_{v,i,j} - f_{v,i,j})/N \quad [16]$$

$$Precision_i = \sqrt{\sum_j (f^*_{v,i,j} - f_{v,i,j})^2/N} \quad [17]$$

where $f^*_{v,i,j}$ and $f_{v,i,j}$ are the estimated and simulated volumes, respectively, for compartment i and voxel j ($j = 1, \dots, N$ where N is the number of simulated voxels). The volume agreement between ground truth and estimates was further assessed by a similarity index called volume overlap (VO) (27) and the total volume agreement (VA) (28). Volume overlap was calculated as

$$VO_{i,j} = \frac{\min\left(f^*_{v,i,j}, f_{v,i,j}\right)}{0.5\left(f^*_{v,i,j} + f_{v,i,j}\right)} \quad [18]$$

Since VO values become unreliable in voxels with low partial volumes, median VO was calculated in binary masks, based on which tissue type contributed the most to each voxel. The VO measure is similar to the Dice coefficient, and assumes total agreement in the spatial distribution of tissues within the corresponding voxels (27), which is true in this case since the simulated data are perfectly aligned with the ground truth. The volume agreement compares the total volume of each compartment, and was defined as

$$VA_i = \left|1 - \frac{\left|\Sigma_j f^*_{v,i,j} - \Sigma_j f_{v,i,j}\right|}{\Sigma_j f^*_{v,i,j} + \Sigma_j f_{v,i,j}}\right| \quad [19]$$

Since the in vivo data included repeated measurements in each subject, the same measures were used to assess the repeatability of the QUASAR-based segmentation, the MPRAGE-based segmentation, as well as agreement between the QUASAR- and MPRAGE-based segmentations. Note, however, that even though SmartExam planning was used (which makes the overall alignment excellent in comparison with manual planning), the interpretation of the measures changes for the in vivo data, since we no longer can compare a ground truth with a perfectly aligned estimate.

Partial Volume Correction Assessment

The impact of the PVC on the CBF quantification was analyzed using statistical tools. Based on all scans, the intra-subject standard deviation (s_w) was calculated for original CBF maps as well as $pCBF_{GM}$ and CBF_{GM}, estimated using both PVC approaches. The corresponding coefficient of variation (COV) and repeatability index ($\sqrt{2} \cdot 1.96 \cdot s_w$) was also calculated. Differences between PVC and conventional smoothing were assessed by analyzing CBF maps convolved with a Gaussian 2D kernel with a FWHM of 5.2 mm. This FWHM was interpolated from the estimated degree of smoothing reported by Asllani et al. (7), based on the number of voxels in the linear regression kernel. The statistical analysis was based on mean values in whole brain GM masks produced by thresholding the GM partial volume maps at 20%. It should be noted that such a low GM threshold would generally not be used for uncorrected perfusion maps and, therefore, we also report some results for a GM threshold of 50%. An example of whole brain GM masks corresponding to GM thresholds of 20% and 50% can be found in Supplementary Material 2.

The dependence of perfusion parameters on the partial volume of GM was assessed by ROI analysis. Mean perfusion was calculated in all voxels within a 10% GM fraction interval (e.g., 70-80%) for uncorrected CBF maps and partial-volume-free CBF_{GM} maps.

PVC could be of particular interest in elderly and in diseases associated with brain tissue atrophy (e.g., neurodegenerative diseases and dementia). In order to obtain an indication of the performance of the proposed method at different stages of brain ageing, the age dependence of the amount of PVE in the data sets was investigated by performing linear regression and Pearson correlation analysis of the ratio CBF_{GM}/CBF as a function of age. The age dependence of CBF, CBF_{GM}, and total GM volume was also analyzed.

Results

The simulation results are summarized in Figure 1. As expected, performance increases with SNR and the mean in vivo whole-brain SNR was 98.6 which make the application to QUASAR data credible. Figure 2 displays segmentation results obtained with the proposed method (QUASAR-based) and the reference method (MPRAGE-based), together with corresponding anatomical references (left column). Note that the anatomical references in Figure 2 also depict the coregistration of the MPRAGE image to the ASL space. The two segmentation methods yielded plausible and overall visually similar tissue volume maps, although clear differences between the two methods can indeed be identified. Figure 3 displays test-retest measures (VA and VO in the session without repositioning) of the QUASAR-based segmentation maps (Fig. 3a-b), the MPRAGE-based segmentation maps (Fig. 3c-d), and comparison between QUASAR- and MPRAGE-based segmentation (Fig. 3e-f). Note that, in one of the sessions, only one MPRAGE scan was performed and the same segmentation result was coregistered to two different ASL scans. Overall, the repeatability was high for both QUASAR- and MPRAGE-based segmentation. The agreement in total volume (VA) and spatial distribution of partial volume estimates (VO) between QUASAR

and MPRAGE was lower than the corresponding intra-method agreements, illustrating the differences in partial volume estimation between the two methods (Fig. 3e-f). The goodness of the in vivo segmentation model fit in terms of mean whole-brain coefficient of determination was (mean±SEM) r^2=0.9994±0.00009. Note that r^2 values should be treated with caution when it comes to nonlinear models, and the value should only be considered as a general indication of the goodness of fit.

Figure 4 displays an example of a PVC result in one subject showing five different parameter maps for each of the two segmentation methods. The two methods produced visually comparable results overall, although with certain apparent differences between the methods, primarily in the CBF_{GM} maps (Fig. 4). Figure 5 shows calculated CBF values in all 40 scans using a GM mask with a threshold of 20%. The corresponding numerical values are presented in Table 1. Quantified GM CBF values are low compared to literature values in uncorrected maps (no PVC), as well as in the $pCBF_{GM}$ maps. PVC-MPRAGE produced somewhat higher CBF_{GM} values than PVC-QUASAR. Mean CBF in GM is displayed as a function of GM volume (10% intervals) in Figure 6. Partial-volume-free CBF_{GM} values produced by PVC-QUASAR were less dependent on GM volume, than those produced by PVC-MPRAGE.

The correction ratio CBF_{GM}/CBF increased with subject age. For PVC-QUASAR, the ratio increased by 0.3% per year (r=0.81, p=0.005) and for PVC-MPRAGE, the increase was 0.4% per year (r=0.63, p=0.05). Neither CBF nor CBF_{GM} showed any significant age dependence, but total GM volume decreased significantly with age. The decrease was 2.40 cm^2 per year (r=-0.89, p=0.0005) for QUASAR-based segmentation, and 1.94 cm^2 per year (r=-0.84, p=0.003) for MPRAGE-based segmentation.

The results from the statistical analysis are summarized in Table 1 (for a GM threshold of 20%). The s_w of GM CBF was lowest for $pCBF_{GM}$ with PVC-QUASAR and highest for CBF_{GM} with PVC-MPRAGE. The uncorrected CBF values showed a s_w value that was lower than CBF_{GM} and similar to $pCBF_{GM}$. However, using PVC-QUASAR, CBF_{GM} and $pCBF_{GM}$ showed a lower COV than the uncorrected CBF. As expected, the session with repositioning was characterized by higher s_w for all parameters, compared to no repositioning. The smoothing generated results similar to the $pCBF_{GM}$ parameter, which is to be expected due to the smoothing effect of the PVC algorithm. PVC-QUASAR resulted in overall lower s_w and COV, compared to PVC-MPRAGE. Although CBF_{GM} had a higher s_w than uncorrected and $pCBF_{GM}$ values, the COV was conserved. The use of a 50% GM threshold did not alter the general conclusions drawn from the statistical analysis (data not shown).

Finally, the different kernel radii yielded different degrees of smoothing, but the mean GM CBF values were the same for all kernel sizes (Supplementary Material 1).

Discussion

Segmentation

The aim of the simulations was primarily to assess the performance of fractional signal-modelling-based segmentation when applied to low resolution data. The results of the segmentation simulation (Fig. 1) suggested that ASL data can be used for robust segmentation and partial volume estimation according to the proposed methodology, assuming that T1 can be reliably estimated. For SNR=100 (similar to in vivo SNR), accuracy was -0.02, 0.004, 0.01 and precision was 0.06, 0.02, 0.04 for GM, WM and CSF, respectively (note that these values are in units of volume fraction, not percentage of the ground truth value). These results are

similar to those of Shin et al. (17), although a saturation magnetization preparation, obviously, results in a lower dynamic signal range than an inversion magnetization preparation. The VA was high overall, in agreement with the accuracy values. The VA values were lowest in CSF, which may be related to the lower amount of voxels with CSF in the digital phantom. A VO above 0.7 has been regarded to be excellent in the literature (29), and although the interpretation of the absolute value is difficult, our results indicate a very high spatial similarity between true and estimated partial volumes. WM had the highest performance overall which is related to the large amount of voxels with high WM fractions. The performance of the segmentation is dependent on the amount of PVE, i.e., a voxel with three different components is generally difficult to segment. It should be noted that the QUASAR sequence is incompatible with fat saturation and this may, in some cases, impair the segmentation results.

One important aspect of the FRASIER segmentation approach is that each tissue type is assumed to have a single T1 value. This type of assumption is common in most segmentation methods employing mixed signal modeling, but it will introduce errors in structures with largely varying T1, for example, in deep gray matter structures. Based on simulations, Shin et al. found that a 10% variation in the T1 of GM yielded a 6.5% error in partial volume estimation of pure GM (17).

The proposed segmentation approach produced realistic segmentation maps in vivo, visually comparable to those obtained with the established segmentation approach (Fig. 2). However, differences are noticeable in all three segmentation maps and, in particular, the QUASAR-based segmentation has sharper boundaries and higher GM volumes. These differences were confirmed when assessing the segmentation agreement through the VA and VO (Fig. 3e-f). Both the QUASAR-based and the MPRAGE-based segmentations showed a high intra-method VA and VO in all subjects (Fig. 3a-d), implying that the repeatability of both segmentation methods was good. The VA between QUASAR and MPRAGE was fair (Fig. 3e), i.e., the total whole-brain volumes were comparable between the two methods. The VO was below 0.9 in all subjects (Fig. 3f) which, as mentioned above, signifies a reduced spatial correspondence of partial volume estimates. This is expected due to the differences in tissue segmentation methodology, but is also partially caused by misalignment (non-ideal coregistration).

Note that the VO calculation assumes perfect alignment (see Analysis section), which is not true for the in vivo case. Although the spatial correspondence is expected to be high through the use of SmartExam, the VO values will be overestimated (27). For the same reasons, in vivo VO values should not be directly compared with the simulation results.

Partial volume correction

The PVC yielded plausible parameter maps with both PVC-QUASAR and PVC-MPRAGE (Fig. 4). The partial tissue perfusion maps $pCBF_{GM}$ and $pCBF_{WM}$ were realistic at visual inspection, and adding them up resulted in an apparently denoised CBF map (cf., last paragraph in the Theory section). Although the two PVC methods generated similar results, PVC-MPRAGE produced more local hotspots (less homogeneity) in the CBF_{GM} map, compared to PVC-QUASAR, especially at the edges of the brain (Fig. 4).

Partial perfusion maps $pCBF_{GM}$ yielded mean GM perfusion values which were slightly lower than the uncorrected and smoothed CBF map. Furthermore, the statistical measures were similar between $pCBF_{GM}$ and the uncorrected maps, of which PVC-QUASAR yielded the lowest variance (Table 1). The observed correspondence between $pCBF_{GM}$ and uncorrected

CBF is expected due to the low perfusion-weighted signal in WM, explained by prolonged blood arrival time and low absolute perfusion compared to GM. That is, for GM perfusion assessment, PVEs due to mixing of WM perfusion signal seems small in our study, although the volumes of different compartments are significant.

The partial-volume-free perfusion maps CBF_{GM}, on the other hand, yielded significantly higher mean GM perfusion values than uncorrected GM CBF, and the PVC-QUASAR and PVC-MPRAGE means were also significantly different (two-sided paired t-test, α=0.05). The mean CBF_{GM} for PVC-QUASAR was 47% higher than the uncorrected GM CBF value, comparable to the results by Asllani et al. who found an approximate increase of 56% in GM voxels with GM volume >20% for a slightly larger voxel size (7). Although it is unlikely for a 20% GM volume mask to be used to estimate GM CBF from uncorrected data, this still gives an indication of the amount of PVE present in the data. For comparison, the 50% GM mask resulted in a 36% higher GM CBF with PVC, also in accordance with previous results. The hotspots mentioned previously were the main reason for the higher mean CBF_{GM} of PVC-MPRAGE (Fig. 5). The hotspots appeared primarily for low partial volumes, which resulted in the decrease of CBF_{GM} with GM fraction seen in Figure 6. Ideally, CBF_{GM} should be independent of the fractional volume of GM, and in this regard our proposed method outperforms the reference method. In fact, our proposed method yields CBF_{GM} values that are almost completely independent of GM volume fraction (Fig. 6).

The amount of PVC was found to be significantly dependent on the subject age. This was found to primarily be an effect of an age dependent decrease in total whole brain GM volume, which also justified the age dependence analysis of our data sets. We observed no significant age dependence of CBF values, with or without PVC, in accord with the previous QUASAR test-retest study (20). Nevertheless, reports of decreased CBF with age are common, and such results should be interpreted with some caution when no PVC has been employed.

One might argue that the existence of a higher spatial gradient (cf., the observed hotspots) is advantageous since it infers less spatial smoothing. However, we used the exact same kernel for the linear regression in PVC-QUASAR and PVC-MPRAGE, and, therefore, the hotspots are more likely related to misalignment and differences in partial volume estimation, than preservation of local flow inhomogeneities. This could very well be the same effect as reported by Chappell et al. who found that imperfections in partial volume estimation and misalignment yielded low GM CBF values for GM volumes >90% (8). Furthermore, CBF_{GM} maps are expected to be independent of GM volume fraction, and PVC-MPRAGE failed to meet this.

To the best of our knowledge, this is the first study using test-retest data to assess the repeatability of partial volume corrected ASL perfusion estimates. The intra-subject standard deviation increased for the partial-volume-free parameters. This is most likely caused simply by the upscaling of the absolute values, since the global COV was maintained (and even slightly decreased for PVC-QUASAR) compared with uncorrected values. The overall increase in intra-subject variance for CBF_{GM} may also be related to imperfections in the partial volume estimation and, for PVC-MPRAGE, coregistration. The intra-subject standard deviation was lowest in the session without repositioning for all parameters. Repeatability was superior for the proposed method compared to the reference method, likely due to the lack of a coregistration step and, possibly, due to more accurate partial volume estimation. Note that one session used a single MPRAGE scan which may have affected the estimated repeatability of PVC-MPRAGE (although coregistration to different ASL scans should mimic a realistic motion between two scans).

Although the global COV was not significantly decreased for partial-volume-free CBF parameters in this study, the local COV is likely to have improved since, in theory, the method segments out CSF and WM which otherwise would cause increased variation on a voxel by voxel basis. Future studies will be focused on repeatability assessment for smaller structures and areas that may benefit from PVC.

Our approach is simplified in that we applied PVC directly on the quantitative CBF maps. This means that differences in GM and WM tracer kinetics (apart from CBF) and tissue properties, such as arterial transit time and relaxation times, are not included. This line of processing was chosen to conserve the main advantage of model-free ASL, namely the lack of need for estimation, or assumption, of bolus length, arterial transit time, tissue relaxation time, brain-blood partition coefficient and the number of compartments. All previous work on PVC in ASL have employed such assumptions, either by using fixed literature values (7,9) or through prior distributions (8).

Petr et al. employed a similar segmentation approach combined with a linear regression (square kernel) PVC to calculate maps of $pCBF_{GM+WM}$ (9). However, they used a separate Look-Locker scan for the segmentation and applied an affine transform to register the data to the ASL images. No partial-volume-free perfusion values were reported, which makes it difficult to compare their quantitative results to ours. Still, the current work and the work by Petr et al. (9) shows that it is possible to perform PVC on ASL data without a high-resolution structural scan. Although these methods employed multi-TI ASL acquisitions, the concept can be adapted to any ASL protocol and sequence, for example a single-TI pCASL sequence, simply by incorporating T1 mapping (preferably within the scan).

In contrast to the square kernel commonly used in spatial linear regression, we employed a circular kernel. We argue that the local region around a voxel is favorably defined by the Euclidian distance. This also reduces the presence of streaky artifacts in the partial-volume-free perfusion maps (cf. (7)). As with square kernels, the smoothing effect of the linear regression increases with kernel size, although the main findings of this study were shown not to depend substantially on the kernel size (Supplementary Material 1).

Although it may be important to remove signal contributions from WM, we argue that the most important PVC in low-resolution perfusion MRI is the removal of the dependence of tissue volume fraction. The importance of disentangling the effects of morphological and haemodynamic alterations cannot be overemphasized. A regional abnormality in estimated perfusion may be sufficient to identify it as a pathological state, but the physiological interpretation of the alteration may be erroneous if PVC is not employed. Furthermore, if both tissue volume and perfusion are affected, differences between groups as well as longitudinal changes may be completely overlooked if PVC is disregarded.

Conclusion

Automatic brain segmentation based on fractional signal modeling was accomplished in the low-resolution ASL CBF space by exploiting the inherent saturation recovery of the QUASAR sequence. The segmentation results were subsequently used for PVC of perfusion maps. Simulations suggested high segmentation performance for realistic data quality, and in vivo segmentation results were comparable to tissue probability maps generated by a reference method. The PVC increased gray matter perfusion values to more realistic levels and the results were most robust for the proposed methodology.

In contrast to previously published methods, the proposed approach produces partial volume estimates based on the same data that perfusion is estimated from, thereby circumventing the need for additional scans and image coregistrations. The implementation was shown to yield superior partial-volume-free GM perfusion estimation, compared to a reference method. We believe that native-space segmentation based on quantitative MRI in connection with perfusion MRI is a promising tool for assessing volumetric dependence of extracted haemodynamic parameters.

Acknowledgements

The authors would like to thank the European COST Action BM1103 on 'Arterial spin labelling Initiative in Dementia' (AID), for promoting networking and collaborative work between research centers. This project was supported by the Swedish Research Council (grant nos. 13514, 2005-6910, 2007-3974 and 2007-6079), the Crafoord foundation, the Lund University Hospital Donation Funds and the Swedish Cancer Society, grant no. 2012/597.

References

1. Detre JA, Leigh JS, Williams DS, Koretsky AP. Perfusion imaging. Magn Reson Med 1992; 23: 37-45.
2. Williams DS, Detre JA, Leigh JS, Koretsky AP. Magnetic resonance imaging of perfusion using spin inversion of arterial water. Proc Natl Acad Sci U S A 1992; 89: 212–216.
3. González Ballester MÁ, Zisserman AP, Brady M. Estimation of the partial volume effect in MRI. Med Image Anal 2002; 6: 389-405.
4. Meltzer CC, Cantwell MN, Greer PJ, Ben-Eliezer D, Smith G, Frank G, Kaye WH, Houck PR, Price JC. Does cerebral blood flow decline in healthy aging? A PET study with partial-volume correction. J Nucl Med 2000; 41: 1842-1848.
5. Erlandsson K, Buvat I, Pretorius PH, Thomas BA, Hutton BF. A review of partial volume correction techniques for emission tomography and their applications in neurology, cardiology and oncology. Phys Med Biol 2012; 57: R119.
6. Hutton BF, Thomas BA, Erlandsson K, Bousse A, Reilhac-Laborde A, Kazantsev D, Pedemonte S, Vunckx K, Arridge SR, Ourselin S. What approach to brain partial volume correction is best for PET/MRI? Nucl Instrum Meth A 2013; 702: 29-33.
7. Asllani I, Borogovac A, Brown TR. Regression algorithm correcting for partial volume effects in arterial spin labeling MRI. Magn Reson Med 2008; 60: 1362-1371.
8. Chappell MA, Groves AR, MacIntosh BJ, Donahue MJ, Jezzard P, Woolrich MW. Partial volume correction of multiple inversion time arterial spin labeling MRI data. Magn Reson Med 2011; 65: 1173-1183.
9. Petr J, Schramm G, Hofheinz F, Langner J, van den Hoff J. Partial volume correction in arterial spin labeling using a Look-Locker sequence. Magn Reson Med 2013; 70: 1535-1543.
10. Ahlgren A, Petersen E, Ståhlberg F, Wirestam R, Knutsson L. Partial volume correction in model-free arterial spin labeling. Proceedings of the 29th Annual Meeting ESMRMB, Lisbon, 2012; 110.

11. Liang X, Connelly A, Calamante F. Improved partial volume correction for single inversion time arterial spin labeling data. Magn Reson Med 2013; 69: 531-537.

12. Petersen ET, Lim T, Golay X. Model-free arterial spin labeling quantification approach for perfusion MRI. Magn Reson Med 2006; 55: 219-232.

13. Parker DL, Christian BA, Goodrich KC, Alexander AL, Buswell HR, Yoon C. Improved accuracy in T1 measurements. Proceedings of the 16th Annual Meeting ISMRM, Sydney, Australia, 1998; 2172.

14. Petersen ET. Brain perfusion imaging: Quantification of cerebral blood flow using ASL techniques. Aarhus: Aarhus University; 2009.

15. Chappell MA, Woolrich MW, Petersen ET, Golay X, Payne SJ. Comparing model-based and model-free analysis methods for QUASAR arterial spin labeling perfusion quantification. Magn Reson Med 2013; 69: 1466-1475.

16. Ahlgren A, Petersen E, Ståhlberg F, Wirestam R, Knutsson L. Using fractional segmentation for estimation of the equilibrium magnetization of arterial blood in model-free arterial spin labeling. Proceedings of the 28th Annual Meeting ESMRMB, Leipzig, 2011; 554.

17. Shin W, Geng X, Gu H, Zhan W, Zou Q, Yang Y. Automated brain tissue segmentation based on fractional signal mapping from inversion recovery Look-Locker acquisition. Neuroimage 2010; 52: 1347-1354.

18. Buxton RB, Frank LR, Wong EC, Siewert B, Warach S, Edelman RR. A general kinetic model for quantitative perfusion imaging with arterial spin labeling. Magn Reson Med 1998; 40: 383-396.

19. Wu O, Ostergaard L, Weisskoff RM, Benner T, Rosen BR, Sorensen AG. Tracer arrival timing-insensitive technique for estimating flow in MR perfusion-weighted imaging using singular value decomposition with a block-circulant deconvolution matrix. Magn Reson Med 2003; 50: 164-174.

20. Petersen ET, Mouridsen K, Golay X. The QUASAR reproducibility study, Part II: Results from a multi-center Arterial Spin Labeling test-retest study. Neuroimage 2010; 49: 104-113.

21. van Osch MJ, Teeuwisse WM, van Walderveen MA, Hendrikse J, Kies DA, van Buchem MA. Can arterial spin labeling detect white matter perfusion signal? Magn Reson Med 2009; 62: 165-173.

22. Young S, Bystrov D, Netsch T, Bergmans R, van Muiswinkel A, Visser F, Sprigorum R, Gieseke J. Automated planning of MRI neuro scans. Proceedings of the SPIE 6144 - Medical Imaging 2006: Image Processing, 2006; 61441M.

23. Aubert-Broche B, Griffin M, Pike GB, Evans AC, Collins DL. Twenty new digital brain phantoms for creation of validation image data bases. IEEE Trans Med Imag 2006; 25: 1410-1416.

24. Donahue MJ, Lu H, Jones CK, Edden RA, Pekar JJ, van Zijl PC. Theoretical and experimental investigation of the VASO contrast mechanism. Magn Reson Med 2006; 56: 1261-1273.

25. Ashburner J, Friston KJ. Unified segmentation. NeuroImage 2005; 26: 839-851.

26. Friston KJ, Ashburner J, Frith CD, Poline JB, Heather JD, Frackowiak RSJ. Spatial registration and normalization of images. Hum Brain Mapp 1995; 3: 165-189.

27. Cardenas VA, Ezekiel F, Di Sclafani V, Gomberg B, Fein G. Reliability of tissue volumes and their spatial distribution for segmented magnetic resonance images. Psychiat Res-Neuroim 2001; 106: 193-205.

28. Liu T, Young G, Huang L, Chen NK, Wong ST. 76-space analysis of grey matter diffusivity: methods and applications. NeuroImage 2006; 31: 51-65.

29. Zijdenbos AP, Dawant BM, Margolin RA, Palmer AC. Morphometric analysis of white matter lesions in MR images: method and validation. IEEE Trans Med Imag 1994; 13: 716-724.

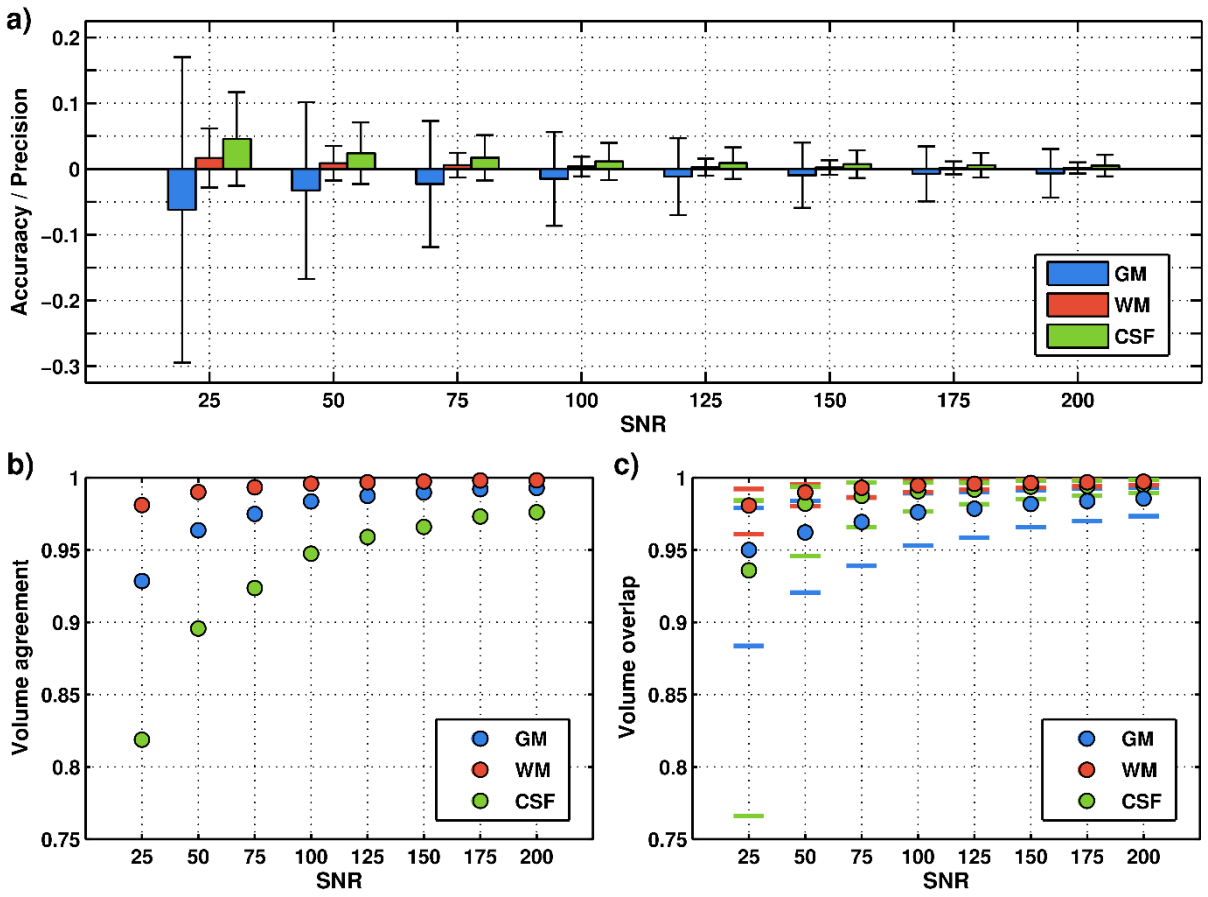

Figure 1. Summary of the performance of the proposed (QUASAR-based) segmentation approach, based on simulations. a) Accuracy (bars) and precision (error bars), according to Eqs. 16-17, as a function of SNR. b) Volume agreement (VA), i.e., agreement in total volume for each compartment (Eq. 19). c) Volume overlap (VO), i.e., median voxel-wise similarity index of the partial volume estimates (Eq. 18), with 1st and 3rd quartiles indicated by bars.

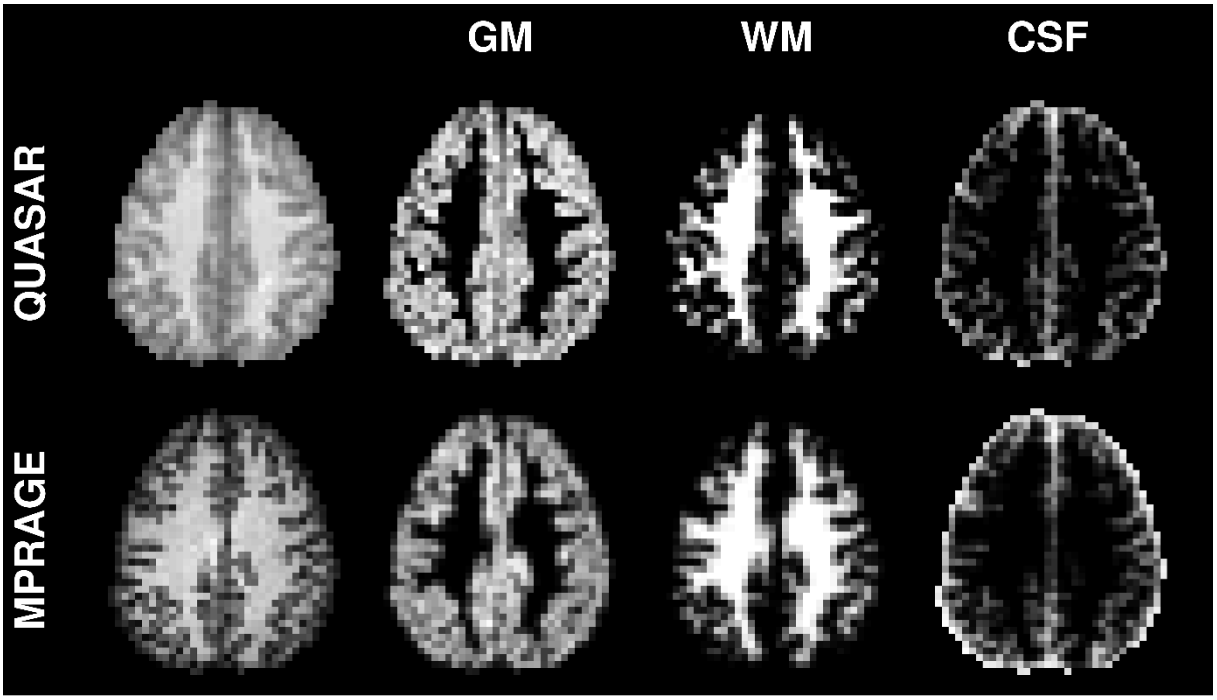

Figure 2. Comparison of segmentation results in one subject. Top row shows segmentation based on QUASAR data, and bottom row shows segmentation results based on the high-resolution MPRAGE scan. The column to the left displays anatomical references, i.e., the QUASAR R1 map and the coregistered T1-weighted MPRAGE image.

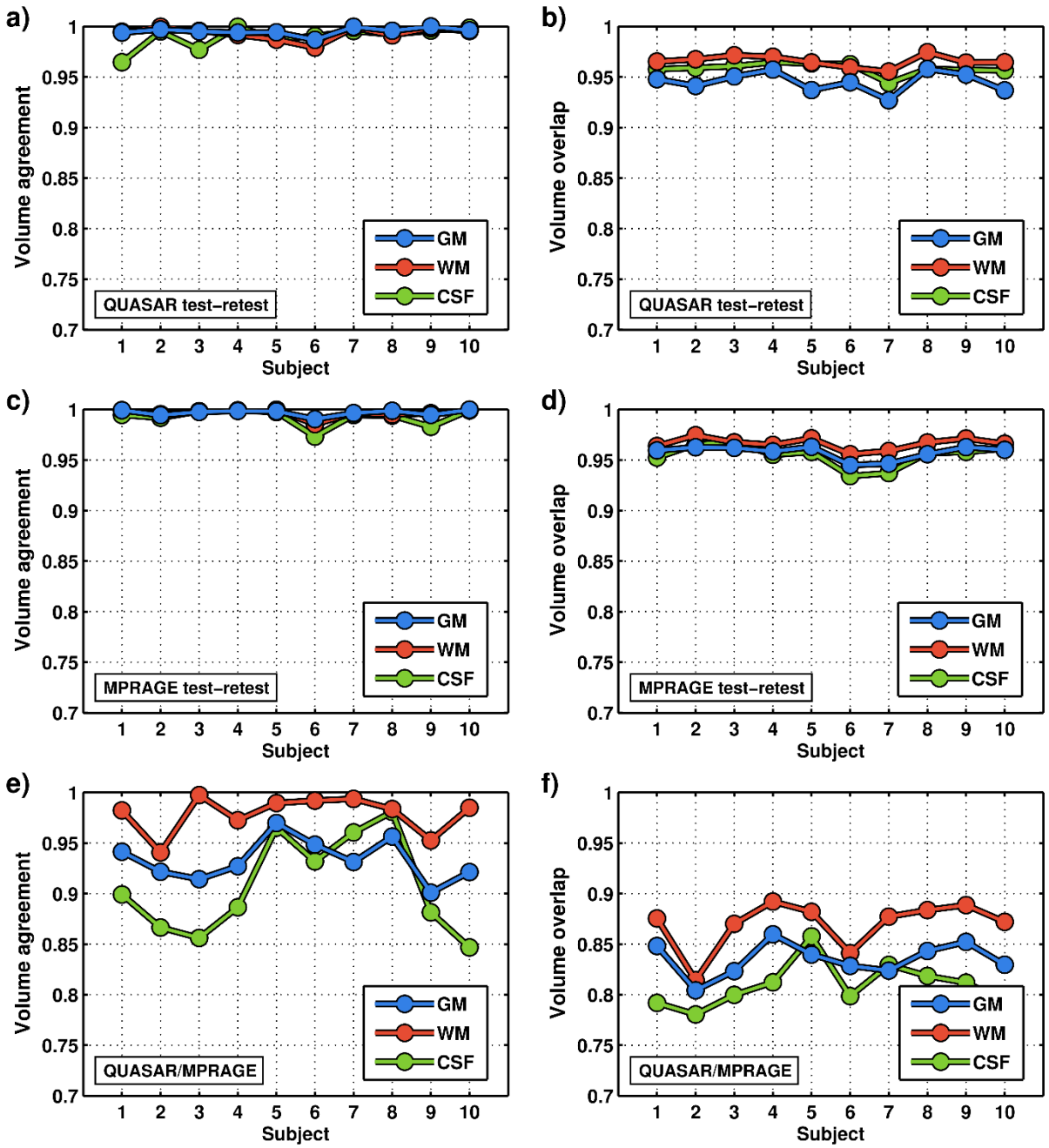

Figure 3. In vivo repeatability results for partial volume estimates (without repositioning) using segmentation based on QUASAR data (a-b), MPRAGE data (c-d), and corresponding comparison of QUASAR and MPRAGE. The left column (a,c,e) displays total volume agreement (VA) for gray matter (blue), white matter (red) and cerebrospinal fluid (green). The right column (b,d,f) displays spatial similarity, i.e., volume overlap (VO) for gray matter (blue), white matter (red) and cerebrospinal fluid (green).

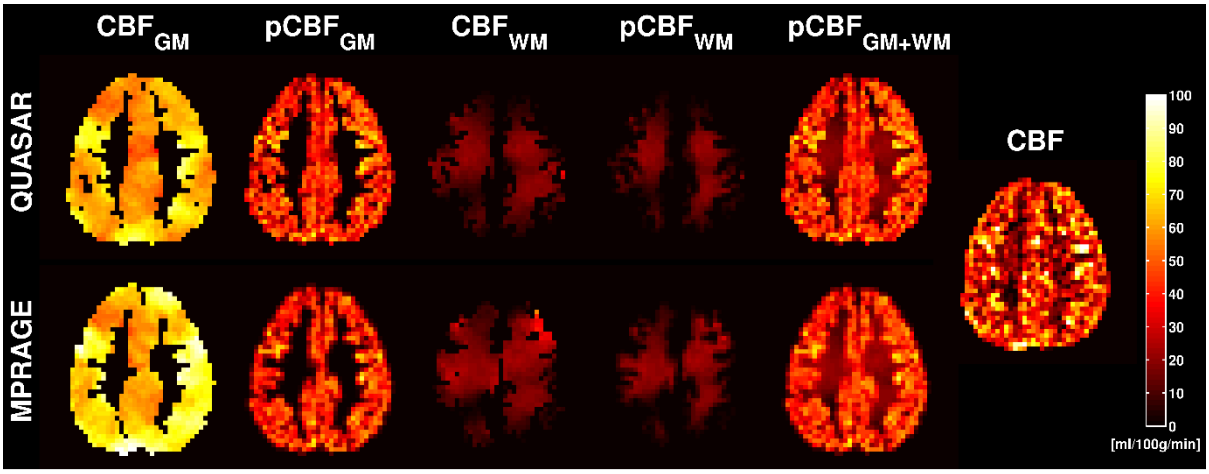

Figure 4. Example of partial volume correction (PVC) results in one subject. The top row corresponds to PVC results based on QUASAR segmentation and the bottom row corresponds to PVC results based on MPRAGE segmentation. CBF_{GM} and CBF_{WM} are tissue volume independent perfusion maps, $pCBF_{GM}$ and $pCBF_{WM}$ are partial tissue perfusion maps (i.e., GM perfusion map without WM contribution, and vice verca), and $pCBF_{GM+WM} = pCBF_{GM} + pCBF_{WM}$. The perfusion map to the right shows the measured CBF. All parameter maps are scaled according to the color bar to the right. CBF_{GM} and CBF_{WM} maps were masked to exclude voxels with partial volumes lower than 10% GM and 10% WM, respectively.

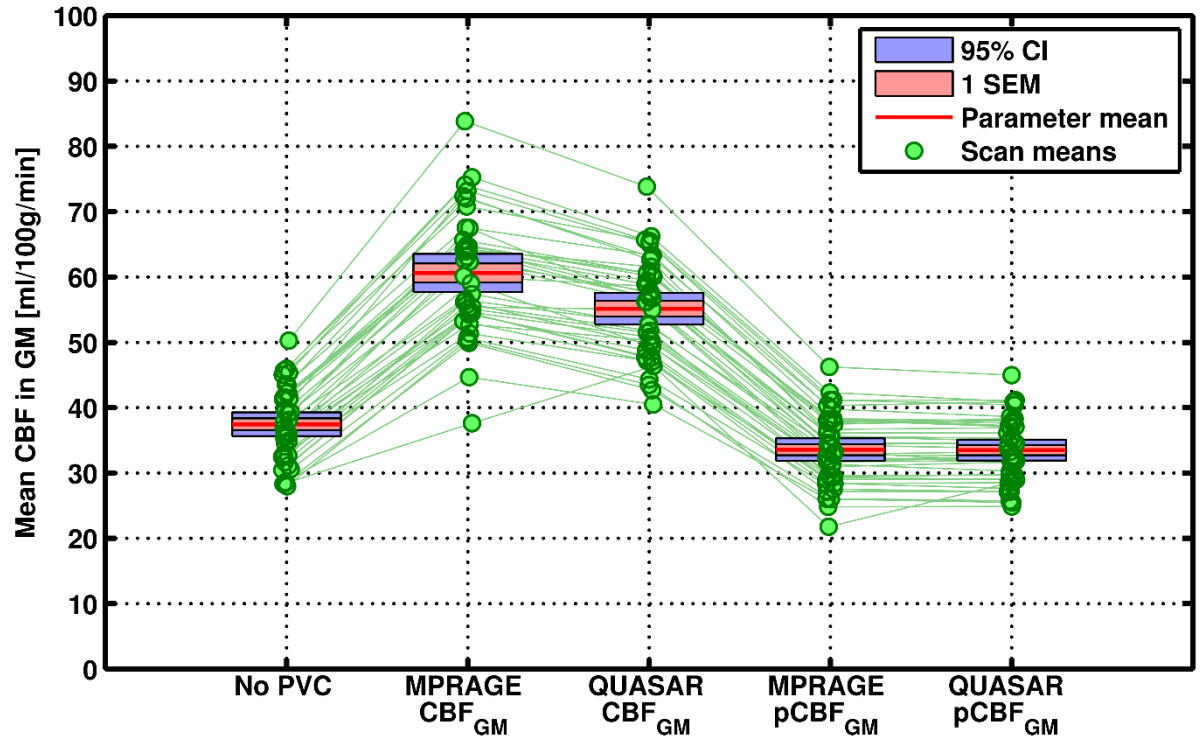

Figure 5. Mean GM perfusion (ROI based on threshold at 20% GM volume) for uncorrected CBF ('No PVC'), volume independent perfusion maps (CBF_{GM}), and partial tissue perfusion maps ($pCBF_{GM}$), for both MPRAGE-based and QUASAR-based PVC. Green dots represents all 40 individual scans, red line shows the mean values (n=40), light red area indicates one standard error of mean (SEM), and the light blue area corresponds to the 95% confidence interval (CI). Each of the 40 scans is connected by a green line.

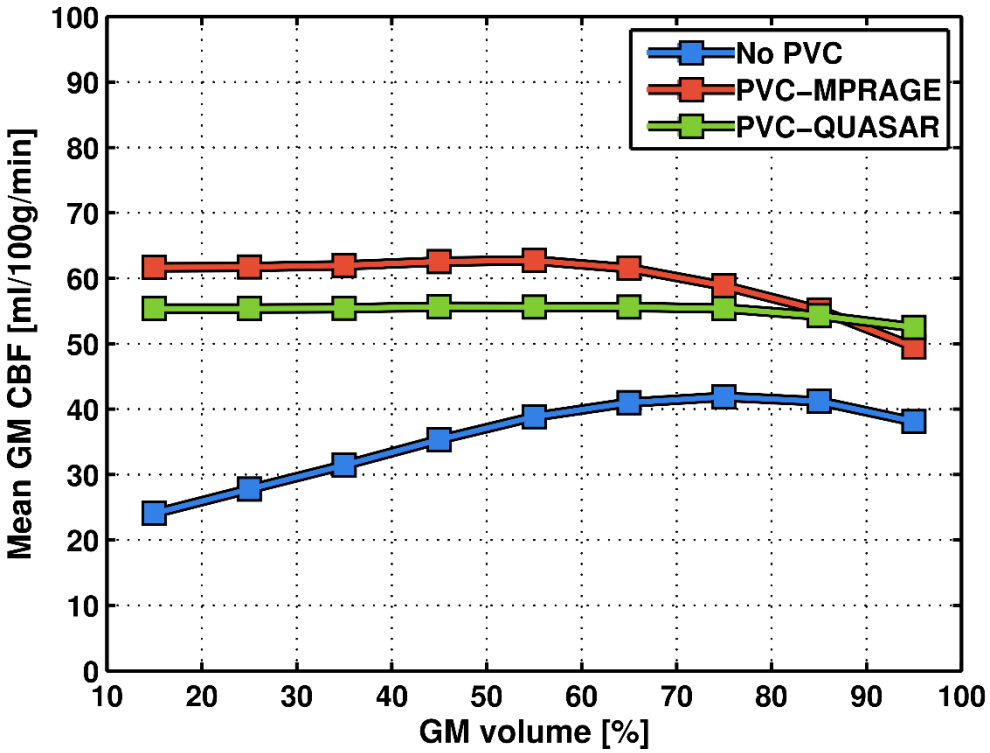

Figure 6. Mean GM perfusion as a function of GM fraction for uncorrected CBF data ('No PVC', blue), and volume independent perfusion maps (CBF_{GM}) using MPRAGE-based (red) and QUASAR-based (green) PVC ($pCBF_{GM}$ is omitted for clarity). Mean values are based on a GM ROI defined as all voxels with a GM fraction within a 10% interval (e.g., an x-axis value of 55% corresponds to the interval 50-60%).

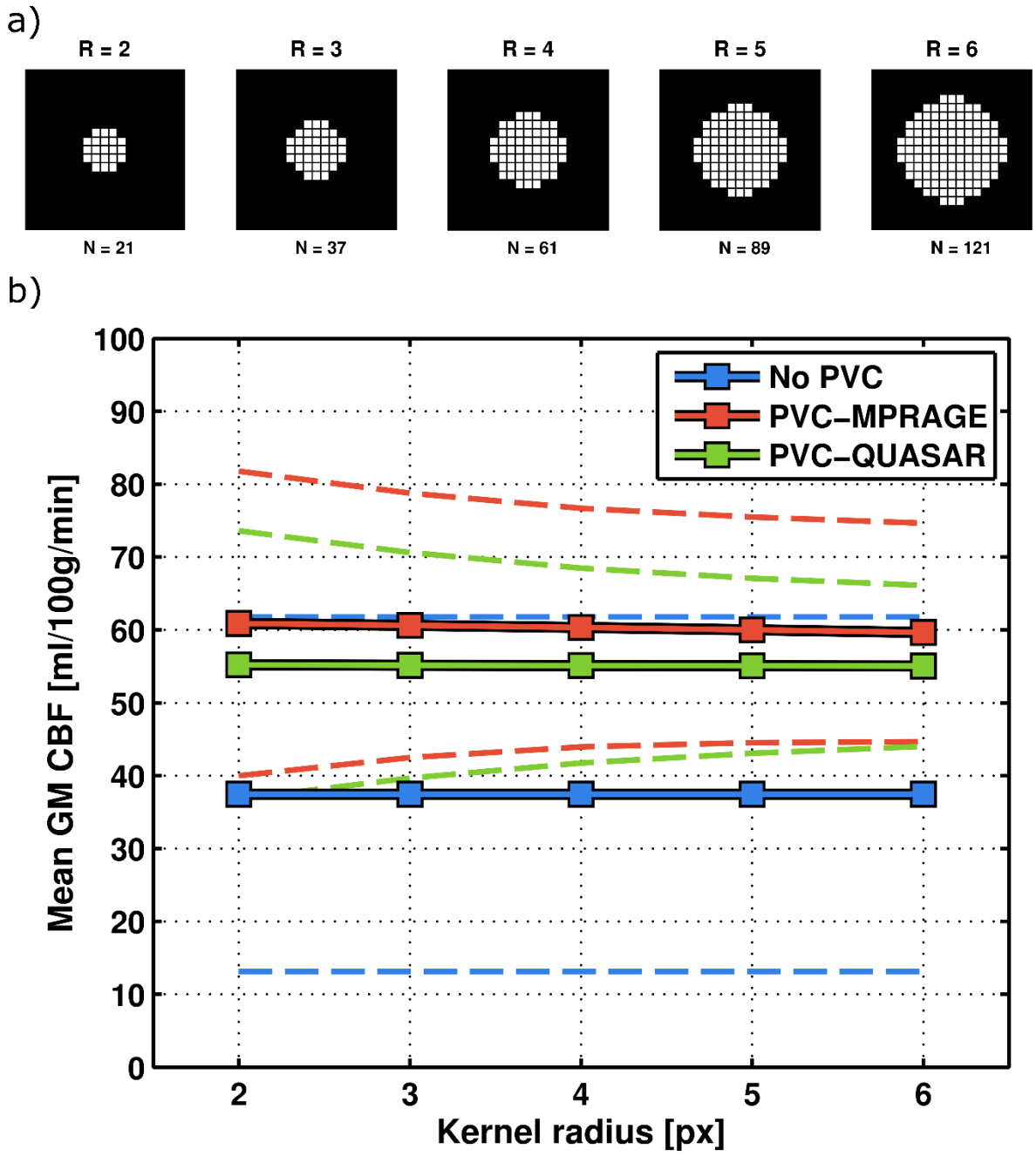

Supplementary Material 1. a) Circular kernels with radii from 2 to 6 voxels. b) In vivo mean CBF in GM without PVC and with the two evaluated PVC methods, including average standard deviations (dashed lines) in the GM mask (i.e., reflecting the degree of effective smoothing), as a function of kernel radius.

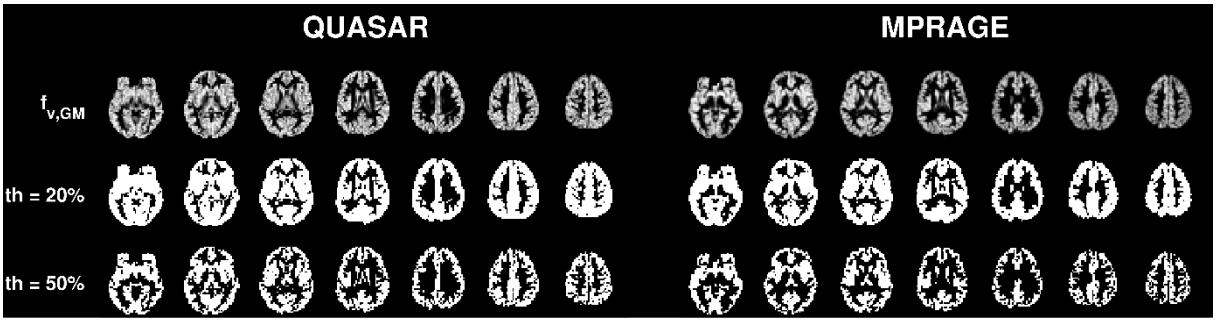

Supplementary Material 2. Example of whole brain GM masks used in the statistical analysis. The left panel shows segmentation using QUASAR data and the right panel shows segmentation using MPRAGE data. The top row displays fractional volume estimation, the middle row shows a whole brain mask with a threshold of $f_{v,GM}$=0.2, and the bottom row shows a whole brain mask with a threshold of $f_{v,GM}$=0.5.

Table 1. Summary of the statistical analysis of the 40 in vivo experiments. All values are based on a binary gray matter mask generated from segmentation maps with a threshold of 20%. SEM is the standard error of mean, s_w is the intra-subject standard deviation and COV is the coefficient of variation.

Parameter	**Mean ± SEM [ml/100g/min]**	**s_w [ml/100g/min]**	**s_w with repositioning [ml/100g/min]**	**s_w without repositioning [ml/100g/min]**	**COV [%]**	**Repeatability index [ml/100g/min]**
CBF (no correction)	37.45 ± 0.90	3.69	3.60	2.69	9.85	10.22
CBF (smoothed)	36.29 ± 0.85	3.58	3.42	2.64	9.85	9.91
CBF_{GM} (MPRAGE)	60.61 ± 1.45	6.76	7.15	4.56	11.15	18.73
CBF_{GM} (QUASAR)	55.14 ± 1.21	5.37	5.02	4.30	9.74	14.88
$pCBF_{GM}$ (MPRAGE)	33.57 ± 0.85	3.48	3.57	2.41	10.36	9.64
$pCBF_{GM}$ (QUASAR)	33.50 ± 0.79	3.18	3.03	2.53	9.49	8.81